

SOLAR ATMOSPHERIC MAGNETIC ENERGY COUPLING: BROAD PLASMA CONDITIONS AND TEMPERATURE SCALES

N. BRICE ORANGE^{1,2}, DAVID L. CHESNY^{1,3}, BRUCE GENDRE^{2,4,5}, DAVID C. MORRIS^{2,4}, AND HAKEEM M. OLUSEYI³

¹OrangeWave Innovative Science, LLC, Moncks Corner, SC 29461

²Etelman Observatory, St. Thomas, United States Virgin Islands 00802

³Department of Physics & Space Sciences, Florida Institute of Technology, Melbourne, FL 32901

⁴College of Science and Math, University of Virgin Islands, St. Thomas, United States Virgin Islands 00802 and

⁵Laboratoire ARTEMIS, Université Côte d'Azur, Observatoire Côte d'Azur, CNRS, boulevard de l'Observatoire, BP 34229, F-06304 Nice Cedex 04, France

Draft version March 1, 2016

ABSTRACT

Solar variability investigations that include its magnetic energy coupling are paramount to solving many key solar/stellar physics problems. Particularly understanding the temporal variability of magnetic energy redistribution and heating processes. Using three years of observations from the *Solar Dynamics Observatory's* Atmospheric Imaging Assembly and Helioseismic Magnetic Imager, radiative and magnetic fluxes were measured from coronal hole, quiet Sun, active regions (ARs), AR cores (i.e., inter moss), and at full-disk scales, respectively. Our feature radiative to photospheric magnetic energy coupling analyses supported a temperature dependence. We present mathematical descriptions of magnetic energy coupling across broad temperature gradients, independent of feature for > 10 G magnetic fluxes. Thus, providing an improved approach for describing magnetic energy redistribution processes of the predominately closed field corona. A general solar atmospheric model is presented that centers on an observationally derived self-similar central engine with possible extension to the cooler atmospheric layers ($\log T \leq 6.0$) of open field structures. Finally, this work indicates stellar X-ray observations can provide insight to currently limited and/or undetectable radiation distributions, and holds potential for understanding their gross atmospheric feature classes thermodynamic profiles.

1. INTRODUCTION

The Sun's atmosphere exists in two phases; one that is magnetically confined near the solar surface and one that consists of the extended atmosphere that interfaces with and comprises the solar wind. The solar atmosphere, observed on the disk and above the limb, can be divided into three distinct regions: active regions (ARs); regions of "quiet" Sun (QS); and coronal holes (CH), i.e., gross feature classes. It has been established that the redistribution of magnetic energy appears to dominate the heating of the corona (e.g., Klimchuk 2015), but the mechanisms responsible for and heights at which plasma heating occurs remain outstanding puzzles.

Solar atmospheric heating of plasmas to coronal temperatures ($\log T \geq 6.0$) is believed to result from the dissipation of magnetic free (i.e., via reconnection events) or wave energy, i.e., such energy conversion events lead to bundles of nanoflare heated loop strands (Parker 1963). However, emerging evidence is challenging the standard coronal heating model, e.g., fast transition region (TR; $4.9 \leq \log T \leq 6.0$) upflows (Tripathi et al. 2012; Orange et al. 2013), and strongly peaked active region core emission measure distributions (Warren et al. 2012).

Throughout the last few decades, extensive work has been carried out on magnetically confined structures (e.g., Aschwanden & Schrijver 2002; Spadaro et al. 2006; Mackay et al. 2010; Orange et al. 2013; Chesny et al. 2013). These works, mainly in relation to the corona, have greatly influenced and enhanced our understanding of solar atmospheric heating (e.g., Aschwanden & Nightingale 2005), and revealed that both steady-state (e.g., Winebarger et al. 2011) and impulsive heating con-

tribute to their generation (e.g., Viall & Klimchuk 2012). Basal heating at cooler atmospheric layers has been implicated as the source and origin of the solar wind, respectively (e.g., Cranmer 2012; McIntosh et al. 2013), which emanates from open field magnetic structures (e.g., Li et al. 2012). Though investigations have sought the existence of a self-similar magnetically open and closed field heating mechanism (e.g., Lee & Magara 2014; Che & Goldstein 2014), little support exists for such (Klimchuk 2014).

Key in pinning down a single dominant solar/stellar atmospheric heating mechanism of closed magnetic field structures is the linear relationship of coronal X-ray luminosity to unsigned magnetic flux (Pevtsov et al. 2003). These results are supported by evidence of self-organized criticality (SOC; Bak et al. 1987), where heating events result from non-linear processes over broad spatial scales (e.g., Lu & Hamilton 1991; Oluseyi et al. 1999b). However, to date, an extension of this radiative to magnetic description across broad electromagnetic spectrum regimes, i.e., visible, ultra-violet (UV), far UV (FUV), extreme UV (EUV), etc., temperature regimes (i.e., photospheric through coronal), multiple epochs of solar activity, and comparisons between large scale open and closed magnetic field structures (i.e., CH versus QS, etc.) remains unexplored.

Constraints on plausible heating mechanism(s) (e.g., Mandrini et al. 2000) can be ascertained from energetic coupling investigations of radiative and magnetic flux (e.g., Fludra & Ireland 2003). That is, observed intensities are dependent on thermodynamic distributions, subsequently governed by heating rates (e.g., Fludra & Ireland 2003; Warren & Winebarger 2006). Importantly,

the established magnetic field strength’s role in heating models indicates much stands to be learned of heating processes, and possibly variations thereof, via gross feature class comparison studies. Notably, under consideration that large thermodynamic gradients (e.g., O’Dwyer et al. 2010) and starkly differing magnetic field geometries (e.g., Orange et al. 2015) should prevail between these features.

ARs are composed of the hottest and densest plasmas (e.g., Del Zanna et al. 2015), across large temperature gradients, and hence, are the most luminous in the FUV, EUV, and soft X-ray. Of interest to ARs is that the most highly energetic transient phenomena in the solar atmosphere, e.g., flares (FL), predominantly occur in their cores, i.e., “inter moss” regions, where plasma of $\log T > 6.3$ resides (Warren et al. 2010; Del Zanna et al. 2015) and densities exceed $\approx 10^{14} \text{ cm}^{-3}$ (O’Dwyer et al. 2010). Note, AR cores (ARCs) reflect the region between the AR’s two opposing magnetic polarity footpoints. Consider, ARC observations favor stable high-temperature emission (e.g., Winebarger et al. 2011), i.e., plasma heating rates much larger than cooling time-scales (Warren et al. 2012), while that of other gross features, and cooler atmospheric layers commonly indicate magnetically confined structures far from equilibrium, i.e., that are characterized by narrow temperature distributions (e.g., Aschwanden & Nightingale 2005; Warren et al. 2008). Thus, it is apparent that gross feature class comparisons, across large temperature gradients, including ARCs, are useful for deciphering the nature of varying plasma heating rates.

In relation to the above presentation, the remainder of this paper is organized as follows. Observational data processing and analysis of gross solar atmospheric feature classes (i.e., CHs, QS, ARs, and ARCs), as well as at full-disk (FD) scales are presented in Section 2. Within Section 3 we present radiative versus magnetic energy measurements (Section 3.1), their linear energetic coupling descriptions, with and without feature dependence (Section 3.2 and 3.3, respectively), and the compilation of the previous results for the development of a theoretical coronal heating model (Section 3.4). Discussion of these results and our conclusions are provided in Sections 4 and 5, respectively.

2. OBSERVATIONS

Observational data was obtained from SDO’s Atmospheric Imaging Assembly (AIA; Lemen et al. 2012) and Helioseismic Magnetic Imager (HMI; Schou et al. 2012) at approximately 3 – 5 day intervals from May 2010 through July 2013. AIA data consisted of the following ten passbands: 94 Å, 131 Å, 171 Å, 193 Å, 211 Å, 304 Å, 335 Å, 1600 Å, 1700 Å, and 4500 Å, which image the Sun’s full disk approximately every 12 s, with the exception of 4500 Å which observes at a typical cadence of ≈ 30 min. These bands observe solar plasma from photospheric to coronal temperatures with a spatial resolution of ≈ 0.6 arcsec pixel $^{-1}$. The HMI data are images of the full disk line-of-sight (LOS) magnetic field with a cadence of 45 s, and spatial resolution of ≈ 0.5 arcsec pixel $^{-1}$. AIA and HMI passband images were pre-processed using standard Solar SoftWare (SSW), with the pointing corrections of Orange et al. (2014a). Rotation effects between pass-

bands were negligible by using observational time differences below AIA’s thermal jitter motion ($\approx 0.''3$; Aschwanden et al. 2011; Lemen et al. 2012; Orange et al. 2014a).

AIA 193 Å images, per observational date, were used to select two CH, QS, ARs and ARCs (e.g., Figure 1). For each selected feature all AIA passband and HMI LOS magnetogram data were aggregated, and the typical radiative and unsigned magnetic fluxes measured, respectively. Errors were propagated using a summation of photon counting statistics, and the standard error on the mean. We note here our investigations of solar atmospheric thermal to magnetic energy coupling are carried out via the common approximation that energy flux is proportional to “data numbers” (DNs; e.g., Wolfson et al. 2000; Benevolenskaya et al. 2002), i.e., AIA data are not calibrated to physical units.

For each observational date the typical solar disk radiative and unsigned magnetic fluxes were also characterized, again with errors propagated as described previously. Note, solar disk radiative and magnetic flux measurements were derived from a region comprising $\approx 95\%$ of the visible disk (i.e., see Figure 1), and hereafter are referred to as our FD feature. Additionally we point out, prior to FD magnetic field characterizations, sunspot regions were masked (i.e., only fluxes $\lesssim |10^5| \text{ G}$ were considered) to minimize downward biasing effects.

3. ANALYSIS & RESULTS

3.1. Radiative Versus Magnetic Energy

In Figure 2 we provide plots of radiative (covering all AIA passbands, with exception of 4500 Å) versus magnetic fluxes (from HMI observations) with respect to our feature set.

Directly comparing Figure 2’s upper coronal results (i.e., 94 Å) to Figure 5b of Benevolenskaya et al. (2002) reveals distinctive similarities. Particularly, that our results align with the suggestions of Benevolenskaya et al. (2002) and Fludra & Ireland (2003) for two differing dependencies of radiative energy versus that of the underlying magnetic field. However, as one progresses to cooler atmospheric layers, i.e., the TR to the chromosphere (171 Å and 304 Å, respectively), our results are reminiscent of the notion of a linear linking of the hot corona to magnetic fields (i.e., Pevtsov et al. 2003).

Though not shown, 4500 Å radiative to magnetic field comparisons provide no evidence of a thermal to magnetic coupling. That is little to negligible variations in its radiative energy occurs for increasing magnetic field strengths, independent of feature. Results consistent with the expected high β (i.e., ratio of gas to magnetic pressure) conditions that should dominate here.

The results shown in Figure 2 reveal as a function of our analyzed features and for solar atmospheric temperatures of $\log T < 4.8$ (i.e., 1700 Å and 1600 Å plots therein), minimal radiative energy distinctions exist. However, there is a slight “knee,” at approximately $\log B \sim 1.0$ where a blending of the radiative energies observed in CH, QS, AR, ARC (to a lesser degree), and FD occurs. We point out that such results are expected again considering the $\beta \gtrsim 1$ conditions that should prevail here (Abbett 2007). In contrast, the ARC results of these regimes are trending towards a possible linear

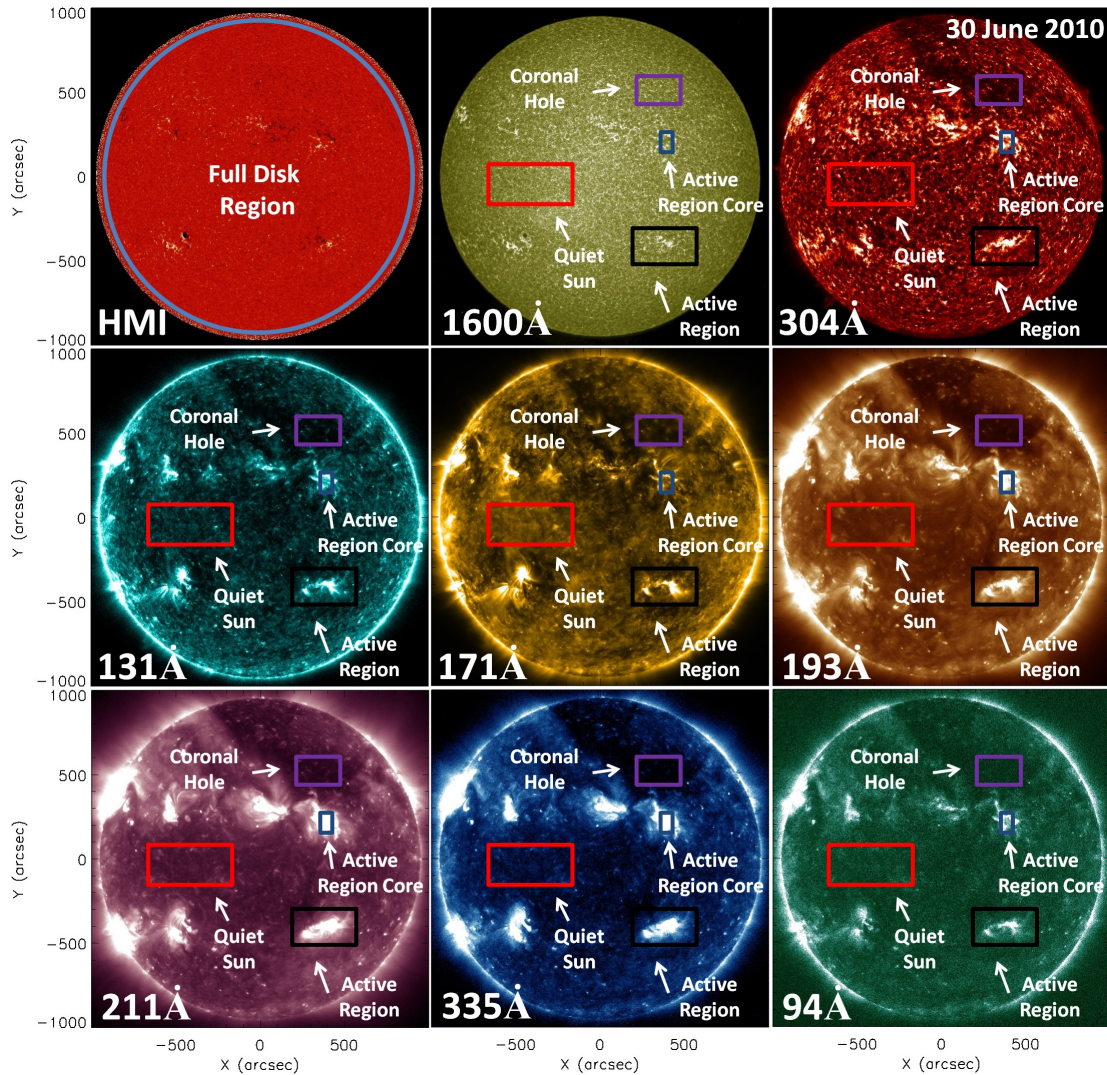


Figure 1. From left to right and top to bottom, respectively, HMI LOS magnetogram, and AIA 1600 Å, 304 Å, 131 Å, 171 Å, 193 Å, 211 Å, 335 Å, and 94 Å radiative images, respectively, observed 30 June 2010. Note, on HMI the circle (blue) indicates the region representing 95% of the solar disk utilized to study the full disk feature reported on herein, while on each AIA radiative image examples of each of the other gross feature classes analyzed herein have been identified.

thermal to magnetic energy relationship (e.g., Pevtsov et al. 2003). Thus, relative to other gross features enhanced ARC photospheric magnetic energies could be leading to frozen-in-flux conditions (i.e., $\beta < 1$) at cooler atmospheric layers/heights.

In the chromosphere, i.e., 304 Å, results are consistent with the expectations of a linear radiative to magnetic energy trend, and shows it scales across the gross feature classes. These results reveal an emerging distinction between observed radiances of CH and QS conditions, which correlate with similar strengths in their underlying magnetic field energies. Note the knee identified in cooler passbands remains distinctly discernable in chromospheric emission.

In passbands dominated by emission from upper TR temperatures (i.e., 131 Å and 171 Å passbands), with the possibility of lower and/or upper coronal contributions (i.e., 131 Å; O’Dwyer et al. 2010; Del Zanna et al. 2011; Schmelz et al. 2013; Boerner et al. 2014), the knee structure of cooler atmospheric layers has “smoothed”

out. However TR radiative versus magnetic energy distributions give rise to signatures of an ankle and knee. The ankle corresponding to CH conditions is distributed downward to lower radiative energies than other studied feature classes. This observation is consistent with suggestions of Pevtsov et al. (2003) for regions dominated by single polarity magnetic fluxes. The knee, emerging where a portion of ARC observations have “migrated” to higher energies, compared to their AR counterparts.

In the middle corona, described here by AIA’s 193 Å and 211 Å passbands ($6.2 \lesssim \log T \lesssim 6.3$; Figure 2), results are generally similar to those of the TR. The only distinction of coronal to TR observations exists in a comparison of their CH and QS radiative energy distributions. Both are characterized by decreased radiative energy distributions relative to other analyzed features. The “upper TR – coronal” ARC knee suggest the possibility of heating not direct attributable to the magnetic field. This idea aligns with recent challenges to the standard coronal heating model interpretation (Parker 1983), particularly,

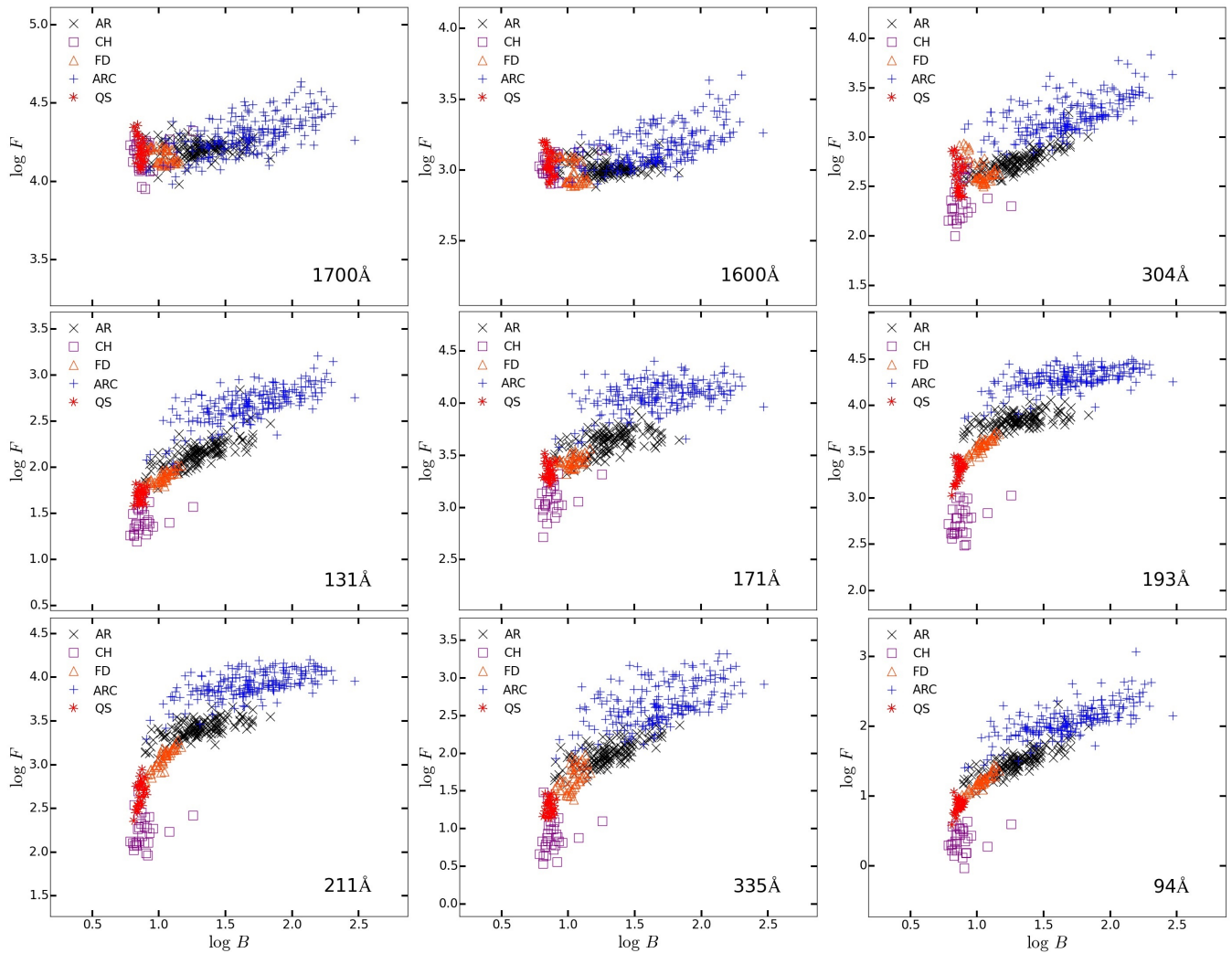


Figure 2. Radiative fluxes (arbitrary units) versus unsigned magnetic flux (arbitrary units) for the 1700 Å, 1600 Å, 304 Å, 131 Å, 171 Å, 193 Å, 211 Å, 335 Å, and 94 Å passbands, from left to right and top to bottom, respectively. On each plot CH, QS, AR, ARC, and FD regions are denoted by *squares* (purple), *asterisks* (red), *x's* (black), *pluses* (blue), and *triangles* (orange), respectively.

observations of inversely proportional emission measure (EM) to underlying field strengths of ARCs (Warren et al. 2012), as well as the absence of non-thermal velocity to temperature trends (Brooks & Warren 2015).

At hotter coronal temperatures, i.e., those of 335 Å and 94 Å observations, similar characteristics prevail to that of the middle corona, and to a lesser degree the TR. In opposition to cooler regions, however, at upper coronal regimes the ARC knee appears smoother. As such a distinct linear relation of QS, FD-R, AR, and ARC features, listed in accordance with increasing magnetic field strengths of the respective distributions, is witnessed. We emphasize, these results, and the previously described upper TR – coronal ARC trend, further elevate arguments for the existence of unresolved coronal emission (e.g., Del Zanna & Mason 2003; Viall & Klimchuk 2012).

3.2. Magnetic Energy Redistribution

In this section linear coupling of magnetic (B) to radiative (F) energies, with gross feature class and AIA passband dependence, is investigated by utilizing the typical

approach, e.g., Golub et al. (1980); Hara (1996); Fisher et al. (1998); Roald et al. (2000); Wolfson et al. (2000); Schrijver (2001); Benevolenskaya et al. (2002); Pevtsov et al. (2003). To that effect, we emphasize, this section serves to provide feature-by-feature comparative discussions of this work to those mined from existing literature.

Per feature, x , i.e., $x \in \{\text{CH, QS, FD, AR, ARC}\}$, and AIA passband, λ , the following linear equation

$$F_{x,\lambda} \propto B^{p_{x,\lambda}}, \quad (1)$$

was fitted to our data to obtain the energetic magnetic to radiative coupling descriptions, i.e., $p_{x,\lambda}$. Prior to discussing our techniques for estimating $p_{x,\lambda}$, we note the 4500 Å observations have been dropped from this analysis, consistent with the report in § 3.1.

Equation 1 coefficients were derived similarly to the methods of Pevtsov et al. (2003). First, a linear least-squares regression fit, carried out *via* the well-known MPFIT (Markwardt 2009) minimization algorithm, was applied as function of x and λ to our observational data set. Additionally, $\langle p_{x,\lambda} \rangle$'s were computed as the average value from the ensemble data sets, with uncertainties prop-

Table 1

Per feature (x) studied in this work, we present power-law indices derived from: all AIA passbands, $\langle p_x \rangle$; AIA's 94 Å passband, $\langle p_{94\text{Å},x} \rangle$; literature mining, p_x^l ; and the subsequent literature reported range (i.e., Min/Max). Note, reported power-law indices have been derived from fits of Equation 1, and are immediately followed by their 1σ deviations.

Feature (x)	$\langle p_x \rangle$	$\langle p_{94\text{Å},x} \rangle$	p_x^l	p^l – Min/Max Range
CH	2.40 ± 0.28	1.96 ± 0.02	$2.06 \pm 0.07^{\dagger 1}$	
QS	1.86 ± 1.18	1.64 ± 0.08	$1.74 \pm 0.21^{\dagger 2}$	0.93/2.03
AR	1.70 ± 0.36	1.15 ± 0.07	$1.43 \pm 0.40^{\dagger 3}$	0.98/2.30
ARC	1.84 ± 0.26	1.47 ± 0.05	—	—
FD	2.15 ± 0.48	1.54 ± 0.04	$1.73 \pm 0.19^{\dagger 4}$	1.47/2.10

^{†1}Pevtsov et al. (2003)

^{†2}Roald et al. (2000); Benevolenskaya et al. (2002); Pevtsov et al. (2003)

^{†3}Fisher et al. (1998); Pevtsov et al. (2003); Fludra & Ireland (2003); Warren & Winebarger (2006); Warren et al. (2012)

^{†4}Wolfson et al. (2000); Pevtsov et al. (2003)

agated from one sigma variances. Subsequently, $\langle p_x \rangle$'s were derived from various samples of passband combinations, i.e., consistent with the boot-strap method (Press et al. 2002), employed on a similar data set by Pevtsov et al. (2003), with errors propagated as one sigma deviations of the various sub-samples.

Negligible $\langle p_{x,\lambda} \rangle$ and $\langle p_x \rangle$ variations were observed between the two analytic approaches; these results are consistent with previous reports (e.g., Pevtsov et al. 2003). Moreover, as discussed below, independent of analysis technique, our x and λ dependent coefficients are consistent with expectations, i.e., all literature mined results. We further wish to emphasize, previous works (e.g., Pevtsov et al. 2003; Warren & Winebarger 2006) have highlighted the importance of two-side significance from zero measurements as a determination of the fit qualities over that of the χ^2 distribution, in radiative to magnetic energy coupling investigations. Deviations from zero of measured two-sided significance between radiative and magnetic fluxes from Spearman's rank correlation coefficients for all our power-law indices were statistically significant (i.e., $s \approx 0$).

Table 1 gives our coefficients, as well as their literature mined counterparts, p_x^l , and range (i.e., $p_{x,min}^l / p_{x,max}^l$). Significant variations of p exist between the subsets, x , as expected, i.e., similar trends exist for p^l subsets. It is recognized our $\langle p_x \rangle$ uncertainties largely reflect statistical properties. However, we point out, as they were derived *via* subset sampling with varying λ dependencies, they also include nonstatistical weighting. Mainly uncertainties associated with varying physical conditions of the solar atmosphere. Nonetheless, it is emphasized, they remain far from being exhaustive, as they are not representative of systematic or selection uncertainties.

In contrast to typical literature, our work embodies $\langle p_x \rangle$ results derived from large solar atmospheric temperature gradients, i.e., λ dependence. Considering the wide literature range reported for various p_x^l 's, and noting no $\langle p_x \rangle$ results, including errors, reported here are grossly disproportionate to expectations, we speculate the possibility of a temperature dependence. Note, our coefficient and reported uncertainties, the latter of which are significantly larger than typical works (e.g., Fisher et al. 1998; Wolfson et al. 2000; Benevolenskaya et al. 2002; Fludra &

Ireland 2003; Warren & Winebarger 2006; Warren et al. 2012), are remarkably consistent with the p_{real} data set of Pevtsov et al. (2003). Of distinct interest then, said data set of Pevtsov et al. (2003) was estimated *via* object averaging of power-law indices under varying physical constraints, in order to provide more realistic errors. Therefore, we feel our results are reasonable approximations to feature coefficients and error estimates, mainly in terms of works executing the typical literature approach as presented here. More importantly, in § 3.3 we address our speculations for a possible temperature dependence embedded within this common linear radiative to magnetic coupling description (i.e., Equation 1).

In terms of the above suggested temperature modulations of power-law indices, we have additionally included 94 Å results in Table 1, where its errors reflect one sigma deviations. This passband was chosen given that its predominant upper coronal origin explicitly correlates with the temperature regime most detailed by existing works. Note, its subset consistencies to literature support arguments for cool and hot emission contamination of said passband as a specific function of gross solar atmospheric feature classes (e.g., O'Dwyer et al. 2010). More importantly, however, it emphasizes consistencies between our work and literature for similarly analyzed electromagnetic spectrum regimes. Similarly, direct comparisons of feature to 94 Å to literature mined coefficients further supports our previous arguments of a possible temperature dependence in radiative to magnetic energy coupling assessments.

3.3. Magnetic Energy Redistribution – Revisited

In this section we carry out an extension study of the work of Pevtsov et al. (2003) that investigates the possible extrapolation of their “universal” X-ray luminosity to unsigned magnetic flux (i.e., Equation 1) to other electromagnetic spectrum regimes of the solar atmosphere. Therefore, it also serves to provide more accurate characterizations of power-law indices as a function of λ , which more explicitly explores the previously suggested solar atmospheric temperature dependencies.

We wish to point out, in line with our previous results the work performed herein avoids 4500 Å observations. Additionally, it will be carried out by “mixing” our

feature observations, and using a lower limit magnetic energy cutoff of 10 G. We further expound upon these analytic criteria as follows. First, the 10 G magnetic energy cutoff reduces undesired mathematical applications to our data, i.e., largely avoids varying constraint diagnostics on clustered data subsets. It also aids in reducing nonstatistical effects from instrumental noise, i.e., avoids influences from LOS magnetic fluxes typical of the noise level (≈ 10 G; A. Sterling 2015; private communication). Note, as observed in Figure 2 below this magnetic, and subsequent radiative, boundary our data is a truncation of a hypothetically complete sample. Therefore, theoretically enforcing this lower limit criteria acts to reduce our mixed observations to a more hypothetically complete sample with a minimized truncation bias. It is emphasized, upper limit energetic stipulations have been avoided, given previous works (e.g., Schrijver et al. 1989; Pevtsov et al. 2003) that have established the validity of linear magnetic energy coupling to other distant stellar sources, i.e., more radiatively and magnetically energetic.

In light of our previous speculations for a possible dependence of radiative to magnetic flux distribution descriptions with chromospheric through coronal plasmas, we have chosen a modified form of Equation 1, as follows,

$$F_\lambda \propto a_\lambda B^{p_\lambda}, \quad |B| > 10 \text{ G} \quad (2)$$

which includes the additional free parameter, a_λ . Thus, Equation 2 includes a temperature dependent energetic “scaling” description. We emphasize, in this section we only characterize coefficients as a function of λ , consistent with our criteria of using a mixed sample data set.

Equation 2 coefficients were derived similarly to the prescriptions of § 3.2, e.g., using a linear least-squares regression fit applied as function of λ . In line with previous arguments we additionally employed methodologies for ascertaining more realistic uncertainties in our a_λ and p_λ coefficients. Specifically, we defined $\langle a_\lambda \rangle$ and $\langle p_\lambda \rangle$ as averages over fits to varying physical constraints of our mixed observational sample. In summary, these coefficients reflect fit applications from inducing various: radiative flux modulations (i.e., $\leq \pm 15\%$), degrees of truncation to upper and lower energetic distributions, and random sub-samples of our mixed data set. In that respect, our reported coefficients and errors include weighting from statistical and nonstatistical properties. In particular, nonstatistical effects related to instrument sensitivity, varying physical plasma conditions, and selection biases. We also wish to note here, consistent with our coefficients in § 3.2, deviations from zero of two-sided significance for all varying sub-samples were statistically significant (i.e., $s \approx 0$).

In Figure 3 the fits of Equation 2 to our data, i.e., $\langle a_\lambda \rangle$ and $\langle p_\lambda \rangle$ per AIA passband, compared to our observed mixed feature radiative and magnetic flux distributions is presented. Note, additionally in this figure, mixed sample features not weighted in our model outcomes have been identified, i.e., those < 10 G are accompanied by a unfilled symbol. As observed the fits are consistent with expectations (notions which have previously been confined to upper coronal temperature regimes, to the best of our knowledge). That is, across broad solar atmospheric spatial ranges radiative fluxes linearly scale with those of the underlying magnetic field.

Figure 4 provides our $\langle a_\lambda \rangle$ and $\langle p_\lambda \rangle$ results versus tem-

perature. For direct comparison of our $\langle p_\lambda \rangle$ results to existing literature, we again smoothed over various passband samples, detailed as follows. First, an upper coronal result of $\langle p_\lambda \rangle = 1.21 \pm 0.08$ (i.e., derived from the 94 Å and 335 Å passbands), is consistent Fisher et al. (1998), i.e., $p = 1.19 \pm 0.04$, for ARs, and the universal data description of Pevtsov et al. (2003), plotted as the shaded (gray) region on Figure 4. For the $4.8 \leq \log T \leq 6.2$ temperature regime, we find $\langle p_\lambda \rangle = 0.89 \pm 0.10$, in agreement with Pevtsov et al. (2003)’s reports for XBPs, QS (no averaging), and dwarf stars. Independent of solar atmospheric temperature (i.e., only for $\log T \geq 4.8$), gives a typical power-law index of 1.0 ± 0.2 . Results favoring self-similar plasma heating of the predominately closed field coronal (e.g., Pevtsov et al. 2003), and elevating evidence for an extension of such to cooler atmospheric layers.

Of distinct interest, is our $\langle p_\lambda \rangle$ temperature distributions indication of a linear correlation, i.e.,

$$\langle p \rangle \propto T^\gamma, \quad (3)$$

where γ would be a proxy for the efficiency of magnetic energy redistribution with temperature. We emphasize Equation’s 3 functional dependence of the efficiency of magnetic energy deposition with thermodynamic conditions are results previously speculated to, e.g., Longcope 1998; Longcope & Kankelborg 1999. It is pointed out, an upper TR – lower coronal dip, “ankle,” is additionally witnessed in the $\langle p_\lambda \rangle$ temperature distribution. Said feature could be reminiscent of the expected upper TR peak in current dissipation per particle (Hansteen et al. 2010; Bingert & Peter 2011), or the previously highlighted EM to underlying magnetic field strength dependence (Warren et al. 2012). However, discussions to such are deferred to the proceeding section.

Finally, in terms of our $\langle a_\lambda \rangle$ temperature distribution, we highlight the following. In regards to its functional form: a high index (“energy”) like tail, correlating with cooler atmospheric layers (i.e., $\log T < 4.8$); upper TR a upturn ($\log T \approx 5.8$); upper TR to lower corona peak ($5.9 < \log T < 6.2$); and decreasing indices at increasingly hotter temperatures ($\log T > 6.3$) exists. The interesting nature of this $a(\log T)$ description, is its resemblance to a “typical” solar atmospheric differential emission measure (DEM) distribution, e.g.,

$$DEM(n_e, T) = n_e^2 \frac{dh}{dT}, \quad (4)$$

with h the LOS coordinate and n_e the electron density (e.g., see O’Dwyer et al. 2010). DEMs provide significant insight regarding solar atmospheric thermal structuring. Thus, we emphasize the existence of such a distribution, obtained for our mixed feature sample, aligns with notions for plasma emission derived from a single mechanism (e.g., Raymond & Doyle 1981; Athay 1981; Oluseyi et al. 1999a). It is also speculated, given the $a(\log T)$ and $p(\log T)$ results obtained here, our work possibly highlights an entanglement of thermodynamic and magnetic energy contributions in strict linear energetic coupling investigations (Equation 1). Particularly for descriptions of broad plasma conditions (i.e., AR vs QS, etc.) and spectrum regimes (i.e., soft X-ray through UV).

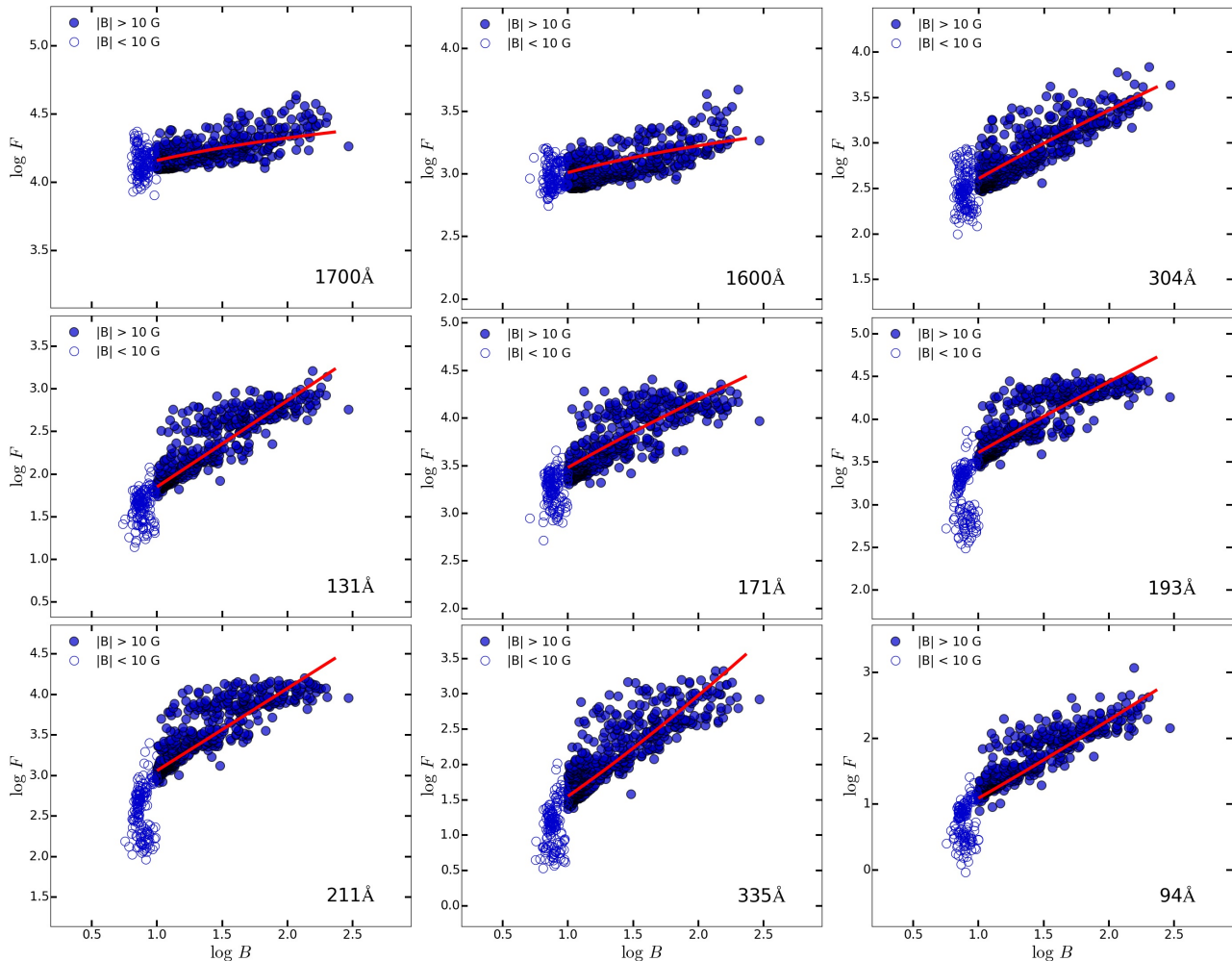


Figure 3. Same as Figure 2, with the feature samples mixed and distinguished by a 10 G magnetic cutoff energy, i.e., < 10 G open (blue circles), and > 10 G shaded (blue) circles. Note, solid (red) line represents the fit of Equation 2 for only observations > 10 G, which is discussed in depth in § 3.3.

3.4. Coronal Heating

Recall, a $\langle p_\lambda \rangle$ upper TR – lower coronal ankle (i.e., $5.8 \lesssim \log T \lesssim 6.3$) was highlighted in § 3.3, that hereafter is referred to as $\log T_w \in (5.9, 6.3)$. Note, $\log T_w$ correlates with TR upturns of our $a(\log T)$ results (Figure 4). We hypothesize, as Equation 3 favors, across the bulk of the solar atmospheric temperature space the efficiency of magnetic energy redistribution approximately linearly scales; assumptions supported by the following. Linear correlations of temperature to EM distributions (e.g., Warren et al. 2012; Del Zanna et al. 2015), and pressure and loop length (e.g., Rosner et al. 1978; Kano & Tsuneta 1995) have been previously established, while evidence for significant $\log T \approx 6.0 - 6.5$ unresolved emission exists (e.g., Del Zanna & Mason 2003; Viall & Klimchuk 2012). Thereby, it’s necessary here to explain the “obscured” $\log T_w$ radiative observations in our magnetic coupling descriptions.

Consider a simplified plane parallel solar atmosphere segmented into cool ($\log T < 5.9$), warm ($\log T_w$), and hot ($\log T > 6.3$) layers (Figure 5), each of which experiences local heating via the freely available magnetic energy (i.e., H_{cool} , H_{warm} , and H_{hot} , respectively; Equa-

tion 3). Cool atmospheric heating, “chromospheric evaporation” E_{cool} (e.g., Fisher et al. 1985; Craig & McClymont 1986; Hansteen et al. 2010), would contribute to warm enhanced plasma emission. Additionally, under the standard coronal heating picture (e.g., Oluseyi et al. 1999a,b), downward conducted hot layer heat flux (C_{hot}) would provide a source of radiatively bright warm emission. Now, assuming for simplicity heated evaporating plasma (E) and conduction (C) processes represent a portion (δ) of local layer heating, the total warm heating (H_{warm}^t) would be given by

$$H_{warm}^t \approx H_{warm} + \delta H_{cool} + \delta H_{hot}. \quad (5)$$

Using similar arguments we arrive at the total cool and hot heating described by

$$H_{cool}^t \approx H_{cool} + \delta H_{warm}, \quad (6)$$

and

$$H_{hot}^t \approx H_{hot} + \delta H_{warm}, \quad (7)$$

respectively (Figure 5). In other words, only warm conduction and evaporation contributes to the cool and hot regions, respectively, while local plus hot and cool energy

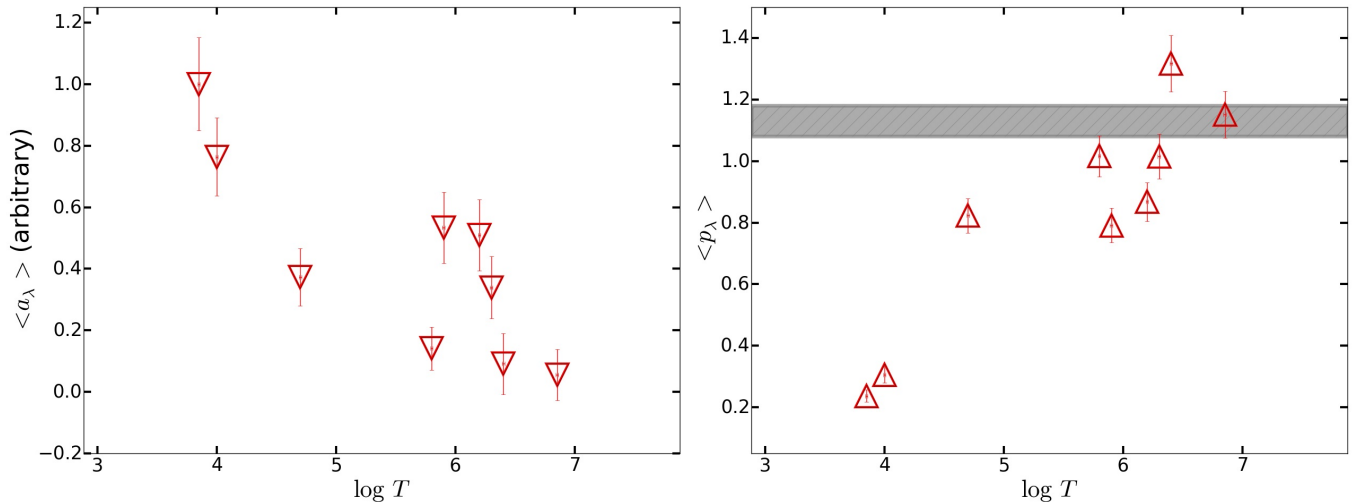


Figure 4. Resultant fit parameters $\langle a_\lambda \rangle$ and $\langle p_\lambda \rangle$, left and right panels, respectively, derived from application of Equation 2 to our mixed feature data set, for observations > 10 G magnetic cutoff energy only (see § 3.3). Shaded gray region on the $\langle p_\lambda \rangle$, corresponds to the “universal” power-law index reported by Pevtsov et al. (2003), i.e., $p = 1.13 \pm 0.05$. Note, we have propagated this “universal” trend across our entire temperature space, as it was derived from only X-ray observations. To that effect, it potentially highlights a source of previously reported variability in linear magnetic to radiative coupling studies as temperature dependence.

redistribution processes contribute to the warm (Figure 5). We find support for these general arguments in works that have favored the presence of unresolved emission, particularly, correlating with our proposed $\log T_w$ space (e.g., Del Zanna & Mason 2003; Viall & Klimchuk 2012; Del Zanna et al. 2015; Warren et al. 2012). We speculate an enhanced volume of warm heated plasma, relative to our other layers, leads to an $\log T_w$ magnetic energy redistribution efficiency ankle. We emphasize, the p versus $\log T$ efficiency ankle as presented here would be expected to manifest as diffuse “unorganized” emission. Below, we expound further upon such arguments.

In terms of the predominantly closed field corona, various scales of closed magnetic flux tubes exist, rooted in the network or intranetwork lanes (Figure 5), and extending to various heights (z) from the solar photosphere (e.g., Oluseyi et al. 1999a,b; Orange et al. 2010, 2011; Tan 2014). The classical one-dimension steady state loop energy equation (e.g., Rosner et al. 1978; Craig & McClymont 1986) can be written in the following conservative form

$$H(T) = \frac{d}{dz} [5n_e v k_B T + F_c] + n_e^2 \Lambda(T), \quad (8)$$

where H defines the energy input (i.e., herein local heating defined previously), and n_e , v , k_B , T , F_c , and $\Lambda(T)$ represent the electron density, velocity, Boltzman constant, temperature, conductive flux, and radiative loss function, respectively. We point out, in Equation 8 the following assumptions have been made. Loops are small compared to the gravitational scale height, such that we can safely neglect gravity. Flows are subsonic, i.e., $v/c < 1$, and low Mach numbers prevail ($M^2 \ll 1$), implying that the kinetic energy density is small compared to the thermal energy density. Finally, we have ignored non-uniformities in loop areas, thus, loop cross section factors have been assumed to be on the order of unity. Note that Equation 8 shows that the energy source (H) supports depletion of enthalpy, heat conduction fluxes, and radiative losses.

The classical Spitzer conductivity for full ionized plasmas is appropriate, i.e.,

$$F_c = -\kappa T^{5/2} \frac{dT}{dz}, \quad (9)$$

with $\kappa \sim 10^{-6}$ for $\log T \geq 5.0$, while for cooler regimes the effects of ambipolar diffusion on the total particle heat flux should be considered (Fontenla et al. 1990, 1991, 1993). The radiative loss function has been analytically approximated by sequenced power laws of the form

$$\Lambda(T) = \Lambda_s (T/T_s)^M, \quad (10)$$

joined continuously (e.g., see Oluseyi et al. 1999a,b). Using the continuity equation,

$$\frac{d}{dz} [n_e v] = 0, \quad (11)$$

and simplifying Equation 8, we arrive at a energy balance form given by

$$H(T) = 5k_B q \frac{dT}{dz} + \frac{dF_c}{dz} + n_e^2 \Lambda(T), \quad (12)$$

with $q = n_e v$. Noting the common solar atmospheric temperature stratification, where

$$\frac{dT}{dz} > 0, \quad (13)$$

for increasing z (e.g., Murawski et al. 2013; Orange 2014), leads to the following condition

$$\left(\frac{dT}{dz} \right)_{warm-cool} \gg \left(\frac{dT}{dz} \right)_{hot-warm}, \quad (14)$$

in relation to our model (Figure 5). In that respect, we consider that conductive (C) and evaporative (E) processes most strongly reflect

$$C \propto \frac{d^2}{dz^2} \left[T^{7/2} \right], \quad (15)$$

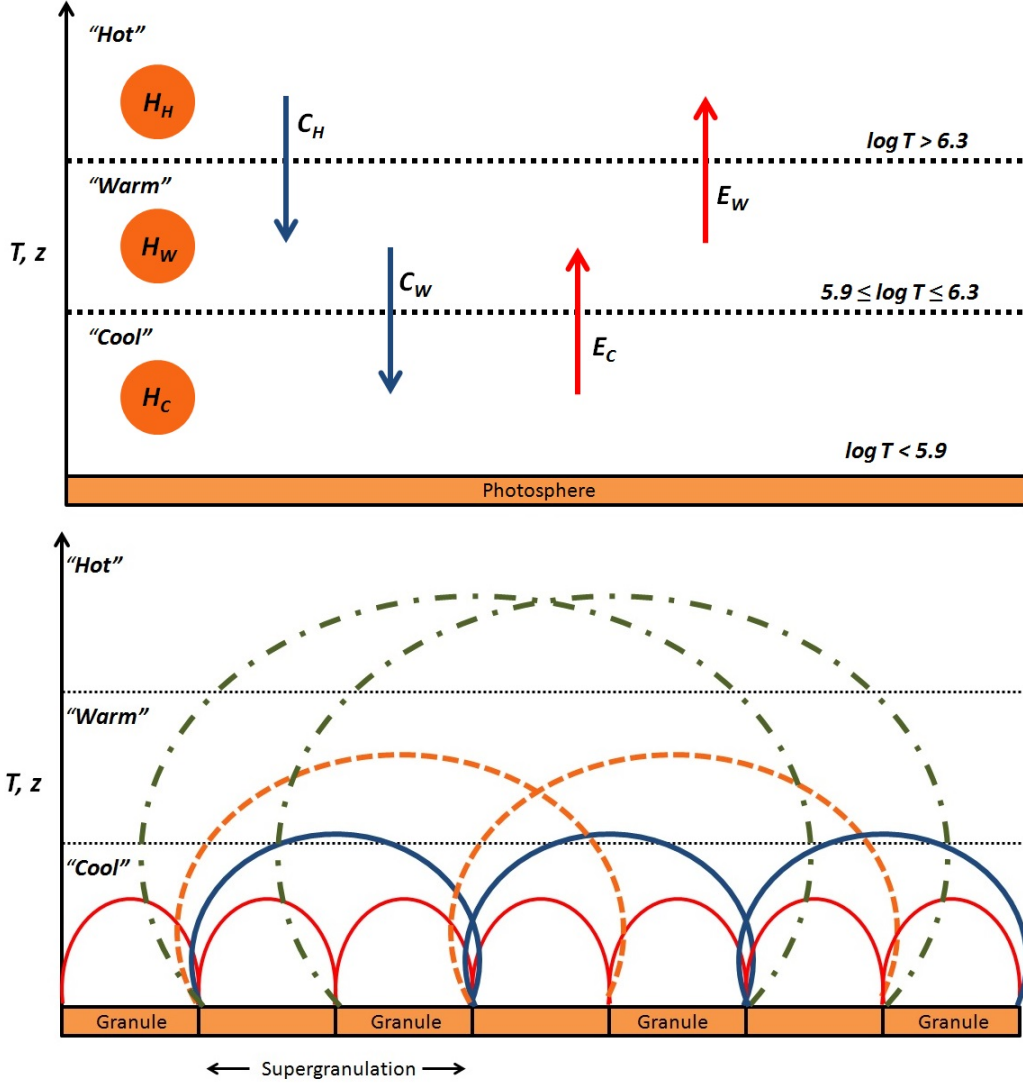


Figure 5. Cartoon schematics of our proposed theoretical solar atmospheric heating descriptions and subsequent energy redistribution processes, as well as their relationship to the predominately closed coronal magnetic field environment.

and

$$E \propto \frac{dT}{dz}, \quad (16)$$

respectively. Directly then Equations 13 – 16 lead to the following conditions

$$H_{hot} > H_{warm} > H_{cool}, \quad (17)$$

thus

$$H_{hot} \gg H_{cool}, \quad (18)$$

while

$$C_{warm} \gg C_{hot}, \quad (19)$$

and

$$E_{cool} \gg E_{warm}. \quad (20)$$

Equations 5 – 7 can then be simplified to

$$H_{hot}^t \sim H_{hot}, \quad (21)$$

$$H_{warm}^t \sim H_{warm} + E_{cool}, \quad (22)$$

and

$$H_{cool}^t \sim C_{warm}. \quad (23)$$

Therefore, arriving at three solutions, “classes,” that should dominate observational signatures in light of our proposed model, i.e., hot local, warm local plus chromospheric evaporation, and cool conductive back heating, for decreasing z , respectively. These solutions lend further support to our previous speculations of the source of the $\log T_w$ magnetic energy redistribution dip. We also emphasize, these results align with the proposed three classes of loop solutions presented by Oluseyi et al. (1999a,b), i.e.,

1. Radiation dominated, where H is large and dT/dz is small,
2. Classical, where both H and dT/dz are intermediate, and
3. Conduction dominated, where H is small and dT/dz is large,

respectively. It is recognized that no discussions were presented in relation to the driver of our hypothesized local heating (H), nor temporal variability, and as such we briefly address these below.

The Sun’s atmosphere is not hydrostatic (Oluseyi et al. 1999a,b), nor does the corona’s mass decrease over time (Hansteen et al. 2010; Guerreiro et al. 2013). Therefore, we would expect time-dependent heating processes, such as postulated here, would lead to near continuous plasma heating/cooling and mass redistribution (Hansteen et al. 2010), e.g., plasma heating driven by field line stress build up and dissipation (e.g., Klimchuk 2006) from photospheric convective motions and magnetic field recycling (Berger 1997; Berger et al. 1997).

Recognizing the presence of knee and ankle structures, and energetic scatter about strict $p_\lambda(\log T)$ descriptions (Figure 3), we would expect additional plasma heating beyond that provided by footpoint motions. For example, the dominant heating mechanism married to a diffuse background component as proposed in recent works (Uritsky & Davila 2014; Tan 2014), and/or plasma heating via magnetohydrodynamic wave dissipation (e.g., Hollweg & Yang 1988; Poedts & de Groof 2004).

Additionally the role of radiative losses in our model discussions have been avoided. Note, radiative loss energy depletion scales as the density squared (Equation 12), while it is widely known n_e decreases for increasing z (Abbett 2007). Shorter cooler loops of our proposed model (Figure 5), characterized by apex densities greater than their hot counterparts (Hansteen et al. 2014), would experience more efficient energy depletion via radiative losses, compared to thermal conduction dominated losses of the longer, hotter, loops (Spadaro et al. 2006; Hansteen et al. 2010; Guerreiro et al. 2013). Thus, in relation to our model, local heating presumably occurs self-consistently across all layers, where progressively cooler atmospheric layers experience more efficient radiative cooling (Abbett 2007; Hansteen et al. 2014).

4. DISCUSSION

Using Equation 1, energetic descriptions, i.e., $\langle p_x \rangle$, were provided for CH, QS, ARs, ARCs, and FD features, i.e., x . In relation to previous literature describing similar magnetic to radiative energy coupling (e.g., Golub et al. 1980; Hara 1996; Fisher et al. 1998; Roald et al. 2000; Wolfson et al. 2000; Schrijver 2001; Benevolenskaya et al. 2002; Pevtsov et al. 2003), our work revealed consistencies to their derived power-law indices, p (Table 1). However, our observations broad electromagnetic spectrum coverage, and subsequent derived energetic coupling coefficients (e.g., $\langle p_\lambda \rangle$ and Equation 2), indicated such consistencies were mainly confined to similarly analyzed portions of the spectrum i.e., soft X-ray.

Importantly, our $p_\lambda(\log T)$ results favored a possible extension of the proposed “universal” relationship between magnetic flux and dissipated coronal heating by Pevtsov et al. (2003) across broad electromagnetic spectrum regimes (i.e., UV – soft X-ray); albeit with modulations to the efficiency of magnetic energy redistribution with temperature (e.g., Equation 3). The potential of such prescriptions are detailed as follows. Note stellar coronae reflect the summation of discrete magnetic elements (e.g., Schrijver et al. 1989). Thus, similar to the conclusions of Pevtsov et al. (2003), our linear radiative

to magnetic energy prescriptions could provide insightful provisions to the field of stellar physics, particularly, in the nature of coronae heating, where current gaps in our knowledge exist from observational limitations. In addition, our observational results for a coupling of magnetic energy deposition efficiency with thermodynamic conditions are of distinct interest, specifically, their potential at yielding new insights to our understanding of fundamental plasma processes (Orange et al. 2014b).

The QS energetic distributions overlap with that of CHs found here (i.e., $\log T \geq 6.0$; Figure 2), could point to presence of self-similar processes leading to open-field structures, i.e., interchange reconnection events resulting in jets (e.g., Yokoyama & Shibata 1995). Speculations consistent with the finds of Orange et al. (2015), whose QS evidence of such energy redistribution events were characterized by differing visibly bright radiative signatures, compared to other gross features, due to the QS large scale magnetic field geometry. Note, due to the general QS geometry, some jets therein are characterized as loop brightenings resultant from opposing horizontal flows (e.g., Shibata et al. 1994; Yokoyama & Shibata 1996). Therefore we hypothesize physical processes attributed to CH formation could be common in QS conditions, where large scale magnetic field geometries lead to radiative observations of more “diffusely” heated plasma. We emphasize, such suggestions align with evidence for the ubiquitous occurrence of solar atmospheric jet phenomena (e.g., Shimojo et al. 1998; Shimojo & Shibata 2000). The predominance of “clustered” QS data points in our observations (e.g., Figure 2), is considered as additional support to such hypotheses (e.g., Pevtsov et al. 2003). More specifically, that is, such distributions decreased evidence for “identical distributions” of the radiative to magnetic fluxes indicates heating beyond the standard flare model (Parker 1963).

The ARC’s upper TR – lower corona knee of radiative to magnetic flux comparisons (i.e., Figure 2) was speculated as an additional heating component not related to the freely available magnetic energy. ARCs nearly linearly related radiative to magnetic energy distribution from lower chromospheric through upper coronal emission could be a result of ubiquitous plasma heating across all solar atmospheric layers, i.e., runaway SOC events. Events that are akin to the coupled diffuse heating component with energy dissipation from SOC-like avalanches (Uritsky & Davila 2014). Interestingly, our ARC knee correlates with the region typically considered as “unresolved” (e.g., $6.0 \leq \log T \leq 6.5$; Del Zanna et al. 2015), where Warren et al. (2012) indicated a switch occurs in EM distributions relation to the underlying magnetic field strength (e.g., see their Figure 9). Thus, our ARC data set is considered supportive to notions for both high and low frequency impulsive heating (e.g., Warren et al. 2012), as well as a challenge to current coronal heating models (e.g., Brooks & Warren 2015). However, as we have only statistically sampled these features, we provide no discussions if such speculations relates to the age of the AR (e.g., see Schmelz & Pathak 2012).

Though our modeled atmosphere (Figure 5) represents extremely generalized descriptions of the complex coronal heating problem (e.g., Klimchuk 2006), we emphasize its alignment with the lukewarm loop model of Oluseyi et al. (1999a,b). Note, their model predicted the ap-

pearance of CHs in the upper TR and corona, network element width with temperature, and TR plasma downflows. Of distinct importance, our work possibly provides a key missing element to the Oluseyi et al. (1999a,b) study – the single dominant generation mechanism (i.e., Equation 3). In addition, it was shown that our model inadvertently led to the three predicted loop class solutions of the Oluseyi et al. (1999a,b) works.

5. SUMMARY

Observational data from all available AIA passbands and HMI LOS magnetograms at approximately 3 – 5 day intervals during May 2010 – July 2013 were utilized to characterize the typical radiative and magnetic fluxes, respectively, of CH, QS, AR, ARCs, and at FD scales. Note these data provided coverage of photospheric (i.e., visible) through upper coronal plasmas (i.e., soft X-ray) of the predominantly open and closed coronal magnetic field environments of the gross feature classes dominating the solar disk, independent of activity phase.

Radiative to magnetic energy coupling assessments were carried out with and without feature dependence. First, with feature (x) dependence by using the typical approach, i.e., Equation 1, to derive their radiative to magnetic energy coupling coefficients, i.e., $\langle p_x \rangle$. These results revealed consistencies to existing literature (Table 1) at similarly analyzed energy ranges (i.e., soft X-ray; Pevtsov et al. 2003), while highlighting a possible temperature dependence in such approaches (§ 3.2). From application of Equation 2 to a mixed feature subsample with a 10 G magnetic energy cutoff, of our original data set, reasonable approximations of magnetic energy redistribution across previously unexplored (to best of our knowledge) temperature regimes were provided (Figure 3). Additionally, these works presented evidence of a linear temperature dependence with magnetic energy redistribution, from chromospheric through coronal regimes (i.e., Equation 3). As such, a simple theoretical coronal heating model was presented in § 3.4.

In relation to this work, we conclude that the combination of our diverse observations, i.e., broad solar atmospheric temperature coverage, *via* AIA passbands, and plasma conditions, of our feature set, with extended time baselines (i.e., ≈ 3 yr), provided the diverse and dynamic range of events from which a simple linear temperature to efficiency of magnetic energy redistribution could be established (Equation 3). Thus, revealing evidence in favor of a single dominant self-similar heating mechanism, mainly of large scale closed coronal field environments. Regardless, as pointed in § 3.4, such assumptions are not considered exhaustive, and the likelihood of other mechanisms contributing to coronal heating remains. These notions align with emerging evidence for an energetic marriage of dominant and diffuse background heating components (e.g., Tan 2014; Uritsky & Davila 2014).

Our work provides support to the expected fundamentally differing heating in regimes dominated by single polarity magnetic flux, i.e., closed versus open field heating (e.g., Pevtsov et al. 2003; Klimchuk 2006). However, from our observations it was speculated that the inferred fundamental difference of open to closed field plasma heating is possibly akin to that of jets and flares (e.g., Shibata et al. 1992; Wang & Sheeley 1993; Wang et al. 1996; Shibata et al. 1997). In that regards this

work further elevates the role of cooler atmospheric studies (i.e., $\log T \leq 6.0$) in identifying the source and origin of CHs, and solar wind mass feeding (Orange et al. 2015). Especially, considering their correlation with heights to where large scale open field structures are considered to originate (e.g., Cranmer 2012).

Our observationally derived dependence of magnetic energy redistribution with temperature (Equation 3) provides the first (to our knowledge) evidence of previously speculated notions, e.g., Longcope 1998; Longcope & Kankelborg 1999. We emphasize, that these results raise interesting prospects for studies detailing similar physical processes under differing plasma conditions (Orange et al. 2014b). Our proposed coronal heating model, founded upon Equation 3, aligned well with the works of Oluseyi et al. (1999a,b), and provided significant provisions to the scope of these studies. Specifically, our work provided the unknown single generation mechanism missing from theirs.

Distinctly interesting to this work is that the average solar DEM is obtained irrespective of gross feature (e.g., Raymond & Doyle 1981; Athay 1981), as well as is appropriate for stars (Antiochos & Noci 1986). Such indicates a single mechanism as the source of plasma emission (Oluseyi et al. 1999a). As revealed here, $a(\log T)$ descriptions were reminiscent to typical solar DEMs (Figure 4). Straightforwardly then, our results favor the presence of a single dominant heating mechanism, while potentially revealing its intimate connection to DEMs. Importantly then, this work casts new light on the utility of narrow-band observations as ad hoc tools for extrapolating solar atmospheric thermodynamic profiles; speculations with far reaching applications to the fields of solar and stellar physics.

This study has addressed SDO’s objective to increase our understanding of the origin of solar activity (Pesnell et al. 2012). In addition, this study has indicated proxies that hold significant potential for the field of stellar physics. Mainly providing possible means for probing distant stellar sources in currently difficult and/or undetectable energy ranges, and techniques for extrapolating radiative to magnetic field characteristics of gross feature classes via unresolved stellar disk observations. Therefore, our work elevates SDO’s extensive data archive as a tool for enhancing our understanding of stellar physics.

6. ACKNOWLEDGEMENTS

A portion of this work has been supported by OrangeWave Innovative Science’s solar physics objective. N.B.O. acknowledges the Florida Space Grant Consortium, a NASA sponsored program administered by the University of Central Florida, grant NNX-10AM01H. N.B.O. and D.L.C. thank the University of the Virgin Islands. B.G. acknowledges financial support from NASA grant NNX13AD28A and NNX15AP95A. Any opinions, findings and conclusions or recommendations expressed in this material are those of the author(s) and do not necessarily reflect the views of NASA. The authors wish to acknowledge P.R. Champy and M. Patel for their assistance in the data processing and collection tasks.

REFERENCES

- Abbett, W. P. 2007, *ApJ*, 665, 1469
- Antiochos, S. K., & Noci, G. 1986, *ApJ*, 301, 440
- Aschwanden, M. J., Boerner, P., Schrijver, C. J., & Malanushenko, A. 2011, *Sol. Phys.*, 384
- Aschwanden, M. J., & Nightingale, R. W. 2005, *ApJ*, 633, 499
- Aschwanden, M. J., & Schrijver, C. J. 2002, *ApJS*, 142, 269
- Athay, R. G. 1981, *ApJ*, 249, 340
- Bak, P., Tang, C., & Wiesenfeld, K. 1987, *Physical Review Letters*, 59, 381
- Benevolenskaya, E. E., Kosovichev, A. G., Lemen, J. R., Scherrer, P. H., & Slater, G. L. 2002, *ApJ*, 571, L181
- Berger, T. E. 1997, PhD thesis, Stanford University
- Berger, T. E., Lofdahl, M. G., Shine, R. A., & Title, A. M. 1997, in *Bulletin of the American Astronomical Society*, Vol. 29, AAS/Solar Physics Division Meeting #28, 896
- Bingert, S., & Peter, H. 2011, *A&A*, 530, A112
- Boerner, P. F., Testa, P., Warren, H., Weber, M. A., & Schrijver, C. J. 2014, *Sol. Phys.*, 289, 2377
- Brooks, D. H., & Warren, H. P. 2015, *ArXiv e-prints*
- Che, H., & Goldstein, M. L. 2014, *ApJ*, 795, L38
- Chesny, D. L., Oluseyi, H. M., & Orange, N. B. 2013, *ApJ*, 778, L17
- Craig, I. J. D., & McClymont, A. N. 1986, *ApJ*, 307, 367
- Crammer, S. R. 2012, *Space Sci. Rev.*, 172, 145
- Del Zanna, G., & Mason, H. E. 2003, *A&A*, 406, 1089
- Del Zanna, G., O'Dwyer, B., & Mason, H. E. 2011, *A&A*, 535, A46
- Del Zanna, G., Tripathi, D., Mason, H., Subramanian, S., & O'Dwyer, B. 2015, *A&A*, 573, A104
- Fisher, G. H., Canfield, R. C., & McClymont, A. N. 1985, *ApJ*, 289, 414
- Fisher, G. H., Longcope, D. W., Metcalf, T. R., & Pevtsov, A. A. 1998, *ApJ*, 508, 885
- Fludra, A., & Ireland, J. 2003, *A&A*, 398, 297
- Fontenla, J. M., Avrett, E. H., & Loeser, R. 1990, *ApJ*, 355, 700
- . 1991, *ApJ*, 377, 712
- . 1993, *ApJ*, 406, 319
- Golub, L., Maxson, C., Rosner, R., Vaiana, G. S., & Serio, S. 1980, *ApJ*, 238, 343
- Guerreiro, N., Hansteen, V., & De Pontieu, B. 2013, *ApJ*, 769, 47
- Hansteen, V., De Pontieu, B., Carlsson, M., et al. 2014, *Science*, 346, 315
- Hansteen, V. H., Hara, H., De Pontieu, B., & Carlsson, M. 2010, *ApJ*, 718, 1070
- Hara, H. 1996, PhD thesis, PhD thesis. *Natl. Astronom. Obs., Japan*. 164 pp., (1996)
- Hollweg, J. V., & Yang, G. 1988, *J. Geophys. Res.*, 93, 5423
- Kano, R., & Tsuneta, S. 1995, *ApJ*, 454, 934
- Klimchuk, J. A. 2006, *Sol. Phys.*, 234, 41
- . 2014, *ArXiv e-prints*
- . 2015, *Philosophical Transactions of the Royal Society of London Series A*, 373, 40256
- Lee, H., & Magara, T. 2014, *PASJ*, 66, 39
- Lemen, J. R., Title, A. M., Akin, D. J., et al. 2012, *Sol. Phys.*, 275, 17
- Li, B., Li, X., & Yu, H. 2012, *Research in Astronomy and Astrophysics*, 12, 1693
- Longcope, D. W. 1998, *ApJ*, 507, 433
- Longcope, D. W., & Kankelborg, C. C. 1999, *ApJ*, 524, 483
- Lu, E. T., & Hamilton, R. J. 1991, *ApJ*, 380, L89
- Mackay, D. H., Karpen, J. T., Ballester, J. L., Schmieder, B., & Aulanier, G. 2010, *Space Sci. Rev.*, 151, 333
- Mandrini, C. H., Démoulin, P., & Klimchuk, J. A. 2000, *ApJ*, 530, 999
- Markwardt, C. B. 2009, in *Astronomical Society of the Pacific Conference Series*, Vol. 411, *Astronomical Data Analysis Software and Systems XVIII*, ed. D. A. Bohlender, D. Durand, & P. Dowler, 251
- McIntosh, S. W., Bethge, C., Threlfall, J., et al. 2013, *ArXiv e-prints*
- Murawski, K., Ballai, I., Srivastava, A. K., & Lee, D. 2013, *MNRAS*
- O'Dwyer, B., Del Zanna, G., Mason, H. E., Weber, M. A., & Tripathi, D. 2010, *A&A*, 521, A21
- Oluseyi, H. M., Walker, II, A. B. C., Porter, J., Hoover, R. B., & Barbee, Jr., T. W. 1999a, *ApJ*, 524, 1105
- Oluseyi, H. M., Walker, II, A. B. C., Santiago, D. I., Hoover, R. B., & Barbee, Jr., T. W. 1999b, *ApJ*, 527, 992
- Orange, N., Chesny, D., Hesterly, K., et al. 2013, *ApJ*, 778
- Orange, N., Oluseyi, H., Bruni, D., et al. 2010, in *Bulletin of the American Astronomical Society*, Vol. 42, *American Astronomical Society Meeting Abstracts #215, #422.03*
- Orange, N. B. 2014, PhD thesis, Florida Institute of Technology
- Orange, N. B., Chesny, D. L., & Oluseyi, H. M. 2015, *ApJ*, 810, 98
- Orange, N. B., Oluseyi, H. M., Chesny, D., et al. 2011, in *Bulletin of the American Astronomical Society*, Vol. 43, *American Astronomical Society Meeting Abstracts #217, #155.10*
- Orange, N. B., Oluseyi, H. M., Chesny, D. L., et al. 2014a, *Sol. Phys.*, 289, 1901
- . 2014b, *Sol. Phys.*, 289, 1557
- Parker, E. N. 1963, *ApJS*, 8, 177
- . 1983, *Geophysical and Astrophysical Fluid Dynamics*, 23, 85
- Pesnell, W. D., Thompson, B. J., & Chamberlin, P. C. 2012, *Sol. Phys.*, 275, 3
- Pevtsov, A. A., Fisher, G. H., Acton, L. W., et al. 2003, *ApJ*, 598, 1387
- Poedts, S., & de Groof, A. 2004, in *ESA Special Publication*, Vol. 575, *SOHO 15 Coronal Heating*, ed. R. W. Walsh, J. Ireland, D. Danesy, & B. Fleck, 62
- Press, W. H., Teukolsky, S. A., Vetterling, W. T., & Flannery, B. P. 2002, *Numerical recipes in C++ : the art of scientific computing*
- Raymond, J. C., & Doyle, J. G. 1981, *ApJ*, 247, 686
- Roald, C. B., Sturrock, P. A., & Wolfson, R. 2000, *ApJ*, 538, 960
- Rosner, R., Tucker, W. H., & Vaiana, G. S. 1978, *ApJ*, 220, 643
- Schmelz, J. T., Jenkins, B. S., & Kimble, J. A. 2013, *Sol. Phys.*, 283, 325
- Schmelz, J. T., & Pathak, S. 2012, *ApJ*, 756, 126
- Schou, J., Scherrer, P. H., Bush, R. I., et al. 2012, *Sol. Phys.*, 275, 229
- Schrijver, C. J. 2001, *ApJ*, 547, 475
- Schrijver, C. J., Cote, J., Zwaan, C., & Saar, S. H. 1989, *ApJ*, 337, 964
- Shibata, K., Nitta, N., Matsumoto, R., et al. 1994, in *X-ray solar physics from Yohkoh*, ed. Y. Uchida, T. Watanabe, K. Shibata, & H. S. Hudson, 29
- Shibata, K., Shimojo, M., Yokoyama, T., & Ohya, M. 1997, in *Astronomical Society of the Pacific Conference Series*, Vol. 111, *Magnetic Reconnection in the Solar Atmosphere*, ed. R. D. Bentley & J. T. Mariska, 29
- Shibata, K., Ishido, Y., Acton, L. W., et al. 1992, *PASJ*, 44, L173
- Shimojo, M., & Shibata, K. 2000, *Advances in Space Research*, 26, 449
- Shimojo, M., Shibata, K., & Harvey, K. L. 1998, *Sol. Phys.*, 178, 379
- Spadaro, D., Lanza, A. F., Karpen, J. T., & Antiochos, S. K. 2006, *ApJ*, 642, 579
- Tan, B. 2014, *ApJ*, 795, 140
- Tripathi, D., Mason, H. E., Del Zanna, G., & Bradshaw, S. 2012, *ApJ*, 754, L4
- Uritsky, V. M., & Davila, J. M. 2014, *ApJ*, 795, 15
- Viall, N. M., & Klimchuk, J. A. 2012, *ApJ*, 753, 35
- Wang, Y.-M., Hawley, S. H., & Sheeley, Jr., N. R. 1996, *Science*, 271, 464
- Wang, Y.-M., & Sheeley, Jr., N. R. 1993, *ApJ*, 414, 916
- Warren, H. P., Feldman, U., & Brown, C. M. 2008, *ApJ*, 685, 1277
- Warren, H. P., & Winebarger, A. R. 2006, *ApJ*, 645, 711
- Warren, H. P., Winebarger, A. R., & Brooks, D. H. 2010, *ApJ*, 711, 228
- . 2012, *ApJ*, 759, 141
- Winebarger, A. R., Schmelz, J. T., Warren, H. P., Saar, S. H., & Kashyap, V. L. 2011, *ApJ*, 740, 2
- Wolfson, R., Roald, C. B., Sturrock, P. A., & Weber, M. A. 2000, *ApJ*, 539, 995
- Yokoyama, T., & Shibata, K. 1995, *Nature*, 375, 42
- . 1996, *PASJ*, 48, 353